Experimental observation of polarization-resolved nonlinear Thomson scattering of elliptically polarized light

Colton Fruhling,* Junzhi Wang, and Donald Umstadter
Department of Physics and Astronomy, University of Nebraska-Lincoln, Lincoln, Nebraska 68588, USA

Christoph Schulzke, Mahonri Romero, Michael Ware, and Justin Peatross†
Department of Physics and Astronomy, Brigham Young University, Provo, Utah 84602, USA

(Received 2 December 2020; revised 26 October 2021; accepted 28 October 2021; published 17 November 2021)

We report experimental results from a study of nonlinear Thomson scattering of elliptically polarized light. Polarization-resolved radiation patterns of the scattered light are measured as a function of the elliptical polarization state of the incident laser light. The relativistic electron trajectory in intense elliptically polarized fields leads to the formation of unique radiated polarization states, which are observed by our measurements and predicted by a theoretical model. The polarization of Thomson scattered light depends strongly on the intensity of the incident light due to nonlinearity. The results are relevant to high-field electrodynamics and to research and development of light sources with novel capabilities.

DOI: 10.1103/PhysRevA.104.053519

I. INTRODUCTION

Thomson scattering (TS) is the scattering of light by free electrons. It is both fundamental and important because of its role as the primary mechanism by which illuminated objects are detectable. TS is governed by the motion of the electrons in the electromagnetic field of the incident light. This motion depends on the intensity, directionality, and polarization of the light. In low-intensity fields, electrons oscillate along the light's electric field at nonrelativistic speeds, and the scattering is linear. In the simple case of linearly polarized incident light, the scattered light is emitted in a dipole-radiation pattern, such as from a linear antenna, and the frequency of the outgoing radiation is nearly identical to that of the incident radiation. As the intensity of the incident light is increased, the electron's motion becomes relativistic, resulting in nonlinear Thomson scattering (NTS). In this nonlinear case, the radiation pattern becomes more complex, and the spectrum of the emitted light develops harmonics.

The theoretical description of an electron's trajectory in an intense laser field was worked out as early as 1935, within the context of quantum-mechanical Volkov states, which are inherently endowed with this behavior [1]. In 1951, Landau and Lifshitz described the trajectory of a classical point electron in an intense plane-wave field in their book *Classical Theory of Fields* [2]. Later, the task of calculating the far-field radiation of the first three harmonics was addressed with a series expansion of the trajectory by Vachaspati [3]. Eberly and Sleeper showed that an electron, initially at rest, acquires a forward drift from the rising edge of a pulse [4]. In 1970, Sarachik and Schappert [5] showed how to calculate all harmonics of radiation in a frame of reference that drifts along with the electron using a Bessel-function expansion. The radiation for an electron with arbitrary initial velocity was calculated by Esarey *et al.* [6] as well as Salamin and Faisal [7].

With the invention of the laser, the achievable intensity of light became high enough to experimentally test these theoretical models for NTS. Englert and Rinehart [8] measured second-harmonic light produced in a head-on collision between an ∼1 keV electron beam and a linearly polarized laser, detected at a 90° angle from the laser propagation; the validity of the measurement was later disputed [9]. Chen *et al.* [10] measured the angular radiation profiles of the second and third harmonics generated by a linearly polarized laser field. Since then, the study of nonlinear Thomson scattering has primarily focused on intense laser fields colliding with relativistic electron beams, frequently referred to as inverse Compton scattering. In those studies, in the laboratory frame, the NTS emerges typically in a narrow pencil-like beam of x rays, making a detailed study of angular emission more difficult. Kumita *et al.* [11] measured the second-harmonic radiation pattern from a relativistic electron beam colliding with a linearly polarized laser in a backscattering geometry. A similar experimental measurement by Babzien *et al.* [12] included a circularly polarized laser, which to our knowledge is the only study of NTS, prior to this work, to employ a laser polarization state other than linear. Jochmann *et al.* [13] measured the spectrally resolved first-harmonic radiation pattern. The transition to studying the extremely nonlinear case has also been studied by multiple groups [14–17]. However, the finer details of the radiation patterns from relativistic electron beams are obscured by the effects of Lorentz transformations.

Previous experimental studies of NTS involved the special cases of either linearly or circularly polarized light. Now, using recently developed experimental methods for polarization-resolved measurements of NTS from low-energy

*colton.fruhling@huskers.unl.edu
†peat@byu.edu

electrons [18], we study NTS with elliptically polarized incident light and compare it with theoretical predictions. In NTS, the electron acquires motion in the direction of the laser wave vector in addition to the motion along the electric field. Our polarization-resolved measurements allow us to decouple electron motion perpendicular to and parallel to the direction of laser propagation. The results help us to improve the current understanding of the interactions of intense light with matter, with applications in both basic physics research and accelerator-driven light sources. Light with unique polarization states is relevant to strong-field photoionization [19], supercontinuum generation [20], nonlinear electrodynamics, and Comptonization of the universe [21–23]. Recent examples of the latter are tests of current theories of cosmology [24] based on measurements of the polarization of the cosmic microwave background, which originated from TS during the expansion of the universe.

In Sec. II, we review the underlying concepts and equations used to understand the experimental results. We describe the experimental setup in Sec. III and proceed to show and discuss the experimental results in Sec. IV. We investigate the transition from a linearly polarized laser field to an elliptically (nearly circularly) polarized laser field. Increased circular symmetry in the laser polarization state leads to increased circular symmetry in NTS emitted out the side of the laser focus. The component of second-harmonic radiation, polarized parallel to the laser propagation, shows a surprising amount of azimuthal asymmetry, which persists from linear to nearly circular polarized laser states.

II. THEORY

We theoretically analyze our results with the help of previous work done by [2,5,7]. In their treatment of the problem of an electron trajectory, they solve the nonlinear motion using a suitable change in variables to the laser phase as seen by the electron $\eta = \mathbf{k}\cdot\mathbf{r} - \omega t$, where ω and $\mathbf{k}$ are the laser angular frequency and wave vector.

For our analysis, we consider a plane-wave laser field traveling along the positive z axis, $\mathbf{A}(\eta) = A_0[\sqrt{1-\delta^2}\sin\eta\hat{x} - \delta\cos\eta\hat{y}]$, where A_0 is the laser vector potential amplitude and δ is a polarization parameter that ranges from zero for linear polarization to $\pm 1/\sqrt{2}$ for circular polarization. We allow A_0 to vary slowly during a pulse that turns on and turns off. For an electron initially at rest, the equation of motion of the velocity contains a component in the direction of the laser polarization that we call the perpendicular component (denoted with $\perp$) and a component in the direction of the laser wave vector that we call the z component. These two components of the motion cleanly separate in the polarization components of the scattered radiation. The velocity equation of motion for an electron, initially at rest and then experiencing the plane-wave pulse described above, is

$$\boldsymbol{\beta}(\eta) = \boldsymbol{\beta}_\perp + \boldsymbol{\beta}_z \tag{1a}$$

$$= \frac{\frac{e}{mc}\mathbf{A}(\eta) + \hat{\mathbf{k}}\frac{1}{2}\left(\frac{e\mathbf{A}(\eta)}{mc}\right)^2}{1+\frac{1}{2}\left(\frac{e\mathbf{A}(\eta)}{mc}\right)^2}. \tag{1b}$$

In the first line, $\boldsymbol{\beta}_\perp$ represents the perpendicular (in the x-y plane) velocity relative to c, which varies on the form of the laser field. $\boldsymbol{\beta}_z$ represents velocity parallel to the direction of the laser propagation. In the second line, e is the charge of the electron, m is the mass of the electron, and c is the speed of light. The nonlinearity of the problem scales with the dimensionless parameter $a_0 = eA_0/mc$. The velocity equation can be integrated or differentiated with respect to time via a chain rule to recover the position or acceleration vectors, respectively, both of which are required to calculate the radiation emitted. It is important to note here that although these equations are simple when parameterized with η, they are quite complex in time and in general contain all harmonics of the laser frequency. For the simple case considered here, with a plane-wave laser field and no initial momentum for the electron, a Fourier transform of Eq. (1b) reveals that the perpendicular component of motion is primarily composed of the odd harmonics, while the z component contains the even harmonics.

The emitted radiation can be calculated with the help of the Liénard-Wiechert potentials and the fields calculated from them [25]. The electric field measured in a particular direction $\mathbf{n}$ from a single electron is described in the far field by

$$\mathbf{E} = \frac{e}{4\pi\epsilon_0}\left[\frac{\mathbf{n}\times[(\mathbf{n}-\boldsymbol{\beta})\times\dot{\boldsymbol{\beta}}]}{(1-\mathbf{n}\cdot\boldsymbol{\beta})^3 R}\right]_{\text{ret}}, \tag{2}$$

where the position, velocity, and acceleration are evaluated at the retarded time $t_{\text{ret}} = t_{\text{detector}} - R/c$ and R is the distance of the particle to the detector. The properties of the scattered light depend on both the electron's trajectory and the direction of observation.

Using Eq. (2), we can expand for a mildly nonlinear case ($a_0 < 1$) and briefly analyze the radiation patterns and polarization. In our experiments, $\mathbf{n}$ is constrained to the transverse direction ($\perp$). In other words, we measure along the equator of the radiation sphere centered on the interaction (shown as a purple sphere in Fig. 3 below) so that $\mathbf{n}\cdot\boldsymbol{\beta} = \mathbf{n}\cdot\boldsymbol{\beta}_\perp$. In this situation, the two orthogonal polarizations of the emitted field, $E_\perp$ in the transverse direction (perpendicular to laser propagation) and E_z in the z direction (along laser propagation), can be separated into different contributions in Eqs. (1a) and (2). We also expand the cubic term in the denominator for small $\mathbf{n}\cdot\boldsymbol{\beta}$ since for the mildly nonlinear case $\mathbf{n}\cdot\boldsymbol{\beta} \leqslant a_0 < 1$. This results in the expressions

$$E_\perp \propto \left[[\mathbf{n}\times(\mathbf{n}\times\dot{\boldsymbol{\beta}}_\perp)] - \cancelto{\text{small}}{[\mathbf{n}\times(\boldsymbol{\beta}_\perp\times\dot{\boldsymbol{\beta}}_\perp)]}\right]\left[1+3\mathbf{n}\cdot\boldsymbol{\beta}_\perp + \mathcal{O}\left(a_0^2\right)\right], \tag{3a}$$

$$E_z \propto \left[[\mathbf{n}\times(\mathbf{n}\times\dot{\boldsymbol{\beta}}_z)] - \cancelto{\text{small}}{[\mathbf{n}\times(\boldsymbol{\beta}_\perp\times\dot{\boldsymbol{\beta}}_z)]} - \cancelto{\text{small}}{[\mathbf{n}\times(\boldsymbol{\beta}_z\times\dot{\boldsymbol{\beta}}_\perp)]}\right][1+\mathcal{O}(a_0)]. \tag{3b}$$

The first term in the large square brackets dominates for each polarization component (unless $\dot{\boldsymbol{\beta}}_z = 0$ for a circular driving field). For linearly polarized laser light, these first terms describe a dipole term orthogonal to $\dot{\boldsymbol{\beta}}_\perp$ for $E_\perp$ and $\dot{\boldsymbol{\beta}}_z$ for E_z. The other terms in the large square brackets also produce dipoles, but they are orthogonal to the respective components of the cross products and make much smaller contributions. For the low-intensity case, $a_0 \ll 1$, the denominator goes to unity. The trajectory in this case contains only transverse motion, and the immediate consequence is that there is no z component in the radiation around the equator, where the experiment is conducted. Thus, explicitly measuring z-polarized light demonstrates the nonlinearity of the interaction. Also, only the first harmonic is present.

At higher intensities, the velocity and acceleration are in the same direction for a linearly polarized field, so Eq. (3a) automatically includes only the first term in the brackets. As previously mentioned, the first harmonic in $E_\perp$ produces a dipole pattern. However, the second harmonic arises primarily from multiplication with the second term in the expansion of the denominator, resulting in $3(\mathbf{n} \times \mathbf{n} \times \hat{\mathbf{e}}_\perp)(\mathbf{n} \cdot \boldsymbol{\beta})$. This can be understood as the multiplication of two orthogonal dipole patterns, resulting in a four-peaked pattern.

Figure 1 shows the fundamental and second harmonics, emitted at various angles in the plane perpendicular to laser propagation, calculated using Eq. (2) and, for comparison, using approximations in Eqs. (3a) and (3b). The agreement between the exact and approximate curves shows that the approximations afford good qualitative understanding of NTS in the moderate relativistic regime. Figure 1 shows NTS for elliptically polarized laser states in addition to linear ones. The second harmonic in E_z grows weaker as the laser polarization approaches circular. In the case of a purely circular laser field, the oscillation in the z direction reduces to zero because the electron is always pushed in one direction by the magnetic field.

One should appreciate that the mixing of harmonics in the denominator plays a significant role, especially at higher intensities. Physically, this can be understood as the wave fronts of the radiation being stretched and compressed from the motion of the electron, which is comparable to the speed of light for a nonlinear laser field. There is an additional coupling of harmonics from the retarded time, which is most significant in the direction of β, but this is not necessary to understand our results.

It is interesting to look at not only the spectrum of the radiation but also the full radiated field as a function of time at a given observation point. Figure 2 illustrates the difference between the linear and nonlinear cases by giving an example of complex polarization states producing TS and NTS. Plotted is the electric field as seen by an observer at 90° from the laser propagation for several laser periods of time. The field is calculated using Eqs. (1) and (2). The linear Thomson scattering case is shown in the top row, which produces linearly polarized scattered light regardless of the polarization state of the laser. The bottom row shows the electric field for a mildly nonlinear laser field and the same elliptically polarized laser states. The laser intensity, the laser polarization state, and the angle of observation can thus be used tailor new radiation sources.

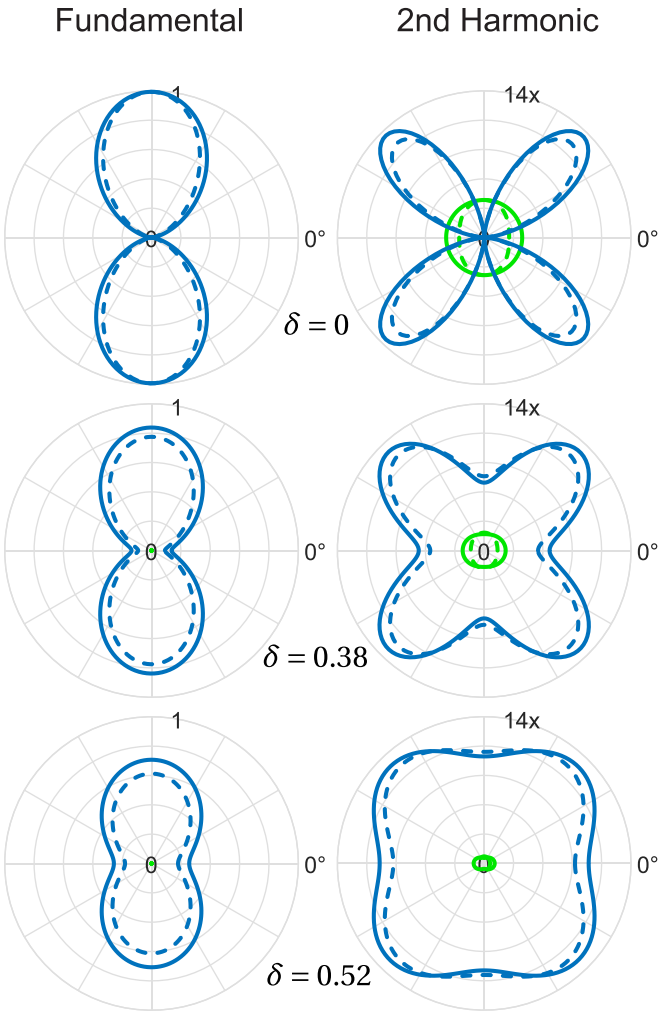

FIG. 1. Calculated radiation patterns for the fundamental (left column) and second-harmonic (right column) NTS with $a_0 = 0.5$ in a plane perpendicular to laser propagation. The calculation is repeated for elliptical laser polarization states $\delta = 0,\ 0.38,\ 0.52$. The dashed lines show approximations in Eqs. (3a) and (3b) (only the first terms in square brackets). The units are arbitrary, but the right column was multiplied by 14 to put it on scale with the left column. Blue lines are for perpendicularly polarized light and green lines are for z-polarized light.

We modeled the interaction of a focused laser with an ensemble average of electrons. We employed the model and code used in Ref. [18]. The electric field is calculated numerically, and the number of scattered photons with the relevant polarization is plotted together with experimental data that we collected. It should be made clear that the model does not assume the same perturbation expansion shown in Eqs. (3b) and (3a), but rather calculates scattered radiation according to Eq. (2). An important feature of the modeling is the effect of electrons being ejected out the sides of the focus while generating NTS. Several different elliptical states were examined which match our experimental conditions: $\delta = 0.14, 0.38, 0.52, 0.59$.

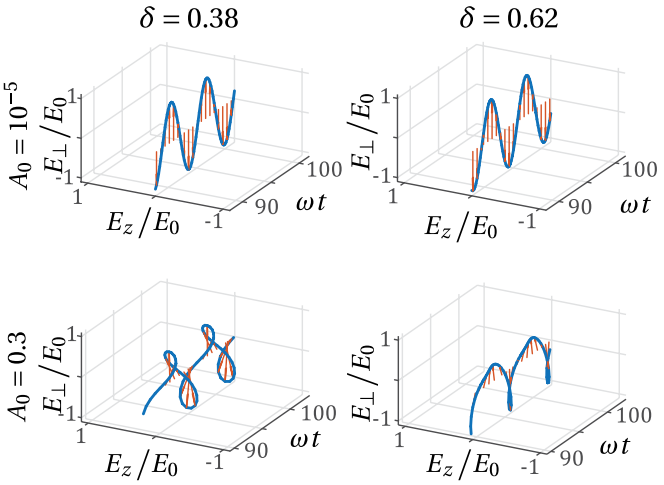

FIG. 2. Calculated radiated electric fields scattered at 90° from the laser propagation. The red arrows are the electric field vector which traces the blue line through time. The top row shows that, for the linear case, the polarization of scattered light is linear regardless of incoming polarization orientation. The bottom row shows complex electric fields generated in a nonlinear interaction.

III. EXPERIMENTAL METHODS

This work was performed at the University of Nebraska–Lincoln's Extreme Light Laboratory with the Diocles laser system. The experimental setup is shown in Fig. 3. A (40 ± 2)-fs laser pulse was generated by a Ti:saphhire chirped pulse amplification (CPA) laser system with a central wavelength of 800 nm and then was focused using an $f/4$ off-axis parabola (OAP). The focal spot size was measured with a microscope objective coupled to a CCD camera. The focal spot radius was measured to be $w_0 = 6.0 \pm 0.4\ \mu$m. The CPA compressor efficiency and input energy were measured to calculate the on-target energy. Based on these measurements, we used relativistic peak field strength $a_0 = 0.76 \pm 0.04$ for scattered first-harmonic measurements and $a_0 = 1.52 \pm 0.08$ for scattered second-harmonic measurements. Immediately before focusing, the beam passed through a quarter-wave plate and a half-wave plate designed for 800-nm light. The quarter-wave plate allowed for control of the ellipticity of the laser, while the half-wave plate allowed for the rotation of the field required to collect the angular radiation pattern. This method was previously utilized by Refs. [10,12]. The polarization was measured after the OAP. We found that the intended quarter-wave plate used in the study was, in fact, approximately a fifth-wave plate. A range of elliptical polarizations were produced and characterized, not including pure circular or linear polarizations.

The laser pulse was focused into a helium-backfilled vacuum chamber. A photon-counting apparatus was designed and implemented first at Brigham Young University and then at Diocles to measure the radiation emitted. The experimental setup for the detection is the same as described in Ref. [18]. The apparatus imaged a 100-μm-long interaction region with a 1:1 lens system, bringing the light out of the chamber via an optical fiber. Prior to entering the lens system, the light was filtered by a linear wire-grid polarizer to discriminate emitted polarization. The polarizer was oriented in two directions during the experiment: the $\perp$ and z directions. The light then passed through a wavelength bandpass filter and was measured by a single-photon counter. The density in the chamber

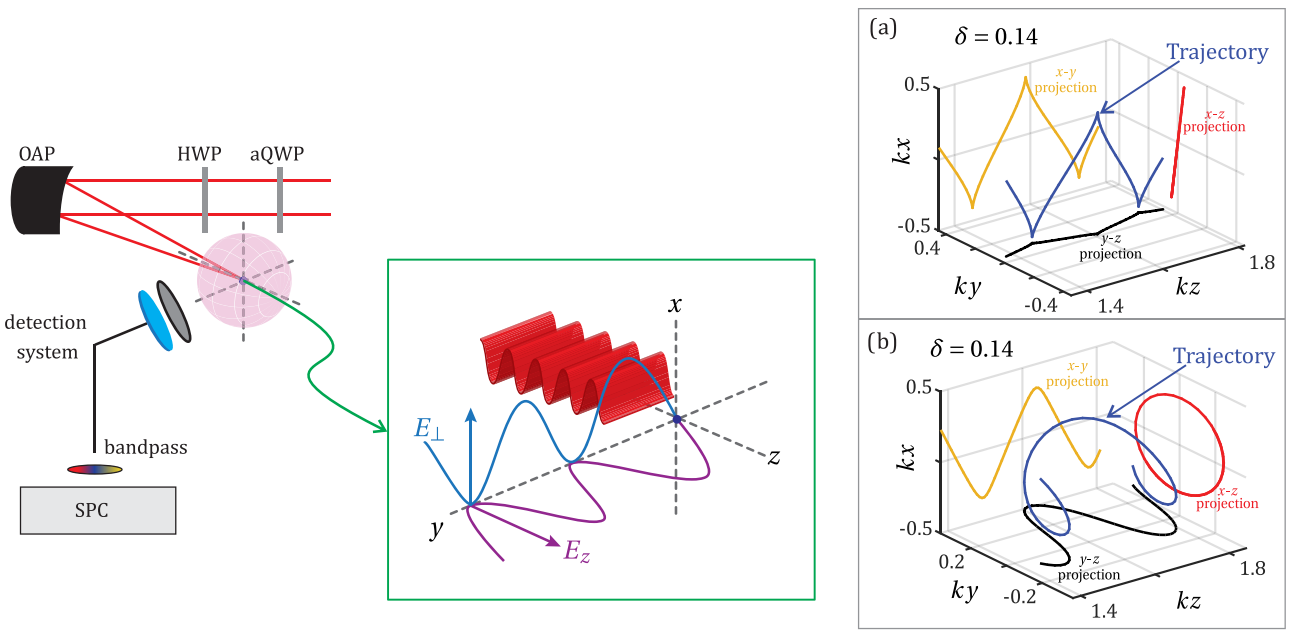

FIG. 3. Experimental setup. A linearly polarized laser pulse passes through an approximate quarter-wave plate (aQWP), introducing an ellipticity in the polarization, then proceeds through a half-wave plate (HWP) to rotate the polarization. The beam was focused into the interaction region with an off-axis parabola (OAP). The scattered radiation is collected at the equator of the radiation sphere by an imaging system comprising a wire-grid polarizer and a 1:1 lens pair. The collection system is coupled to an optical fiber, where the signal is guided through a bandpass filter and then into a single-photon counter (SPC). The interaction geometry and coordinate system is displayed in the center. Insets (a) and (b) show the electron 3D trajectory for a single cycle of the laser in blue, with respective ellipticities. The labeled yellow, red, and black curves are projections along the x-y, x-z, and y-z planes, respectively. The axes are scaled to the laser wave vector $\boldsymbol{k}$.

was adjusted to ensure single-photon counting statistics were achieved. In order to minimize background counts from the long-lived signal, the single-photon counting device was gated to collect only within an instrument-limited 2-ns window of the pulse's arrival at the focus. By measuring the prompt signal, long-lived recombination noise was minimized.

During our measurement of the first harmonic, we introduced helium into the chamber (to donate electrons) until we detected about one photon per 10 laser shots on average in the 2-ns window. The backing pressure of helium was measured to be 1.03×10^{-3} Torr. The laser energy was set to 40 ± 3 mJ on target and focused to a (6 ± 0.4)-μm spot size (FWHM). The solid angle of the collection system is $\approx 0.6 \pm 0.07\,\pi$ sr. Taking these factors into account, we approximate the average cross section of the interaction to be $\approx 1.04 \pm 0.18 \times 10^{-24}\text{cm}^2 = 1.57 \pm 0.26\sigma_T$, where σ_T is the Thomson cross section. In addition to the radiation patterns shown below, this result supports the assumption that TS was the primary phenomenon observed.

The first harmonic was measured with a bandpass filter centered at 900 nm with 40-nm bandwidth, and the second harmonic was measured with a bandpass filter centered at 450 nm with 40-nm bandwidth. These redshifted fundamental and second harmonics correspond to redshifting induced by a laser with $a_0 = 0.5$. Although the peak field in the focus exceeds this, much of the focal volume is in this range. The laser energy was increased for the second-harmonic data while keeping the focal spot size the same for both data sets. The spectral filtering affects the amount of laser focal volume that is measured because there are more electrons that experience a laser intensity of $a_0 = 0.5$ for the second-harmonic data set compared to the first-harmonic data set. The second-harmonic data set is also subject to somewhat stronger ponderomotive effects.

We measured both the first- and second-harmonic radiation patterns for multiple polarization states from near-linear polarization to near-circular polarization of the light. Each polarization state is characterized by the parameter δ described in Sec. II. These are specified for each graph shown in Figs. 4, 5, and 6.

To better appreciate the radiation patterns, single-cycle electron trajectories for near-linear and near-circular driving fields are shown on the right side of Fig. 3. The blue curves show the trajectories scaled by the laser wave vector $\boldsymbol{k}$ in three-space, while the yellow, red, and black curves show the projections of the trajectory on the x-y, x-z, and y-z planes, respectively.

IV. RESULTS

The evolution with ellipticity of the first-harmonic radiation pattern for perpendicularly polarized light is shown in Fig. 4. For each polarization state, the number of photons emitted in each direction within a plane perpendicular to laser propagation is shown. Rather than rotate the detector, the half-wave plate shown in Fig. 3 was used to rotate the axes of the elliptical polarization states, which in principle accomplishes the same thing. The theoretical calculations are scaled to match the number of photon counts received from 1000 laser shots, using a single overall scaling factor for all

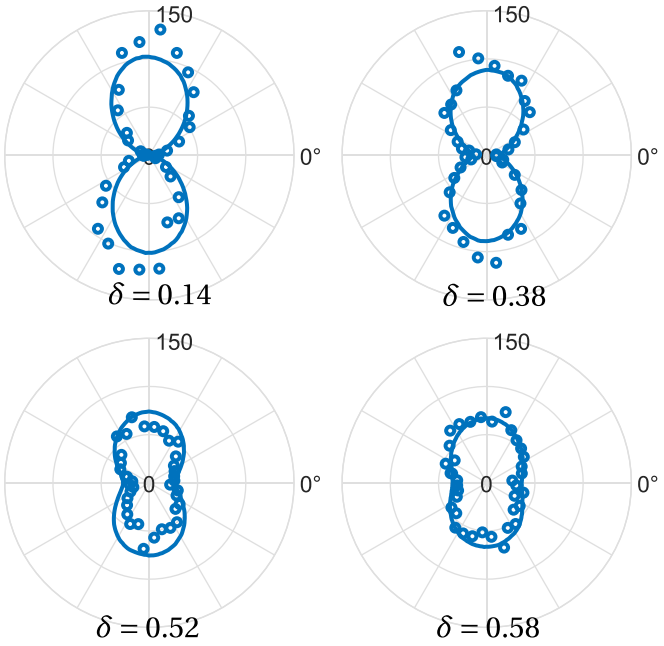

FIG. 4. Number of photons counted per 1000 laser shots in the wavelength range 900 ± 20 nm emitted in the plane perpendicular to laser propagation. Measurements of $\perp$ polarization for different elliptical laser polarization states are shown, all with peak laser field strength $a_0 = 0.76 \pm 0.04$. The data are compared with theoretical simulations (solid line) using the model described in Ref. [18] with an ensemble of 10 000 electrons randomly positioned in the laser focus.

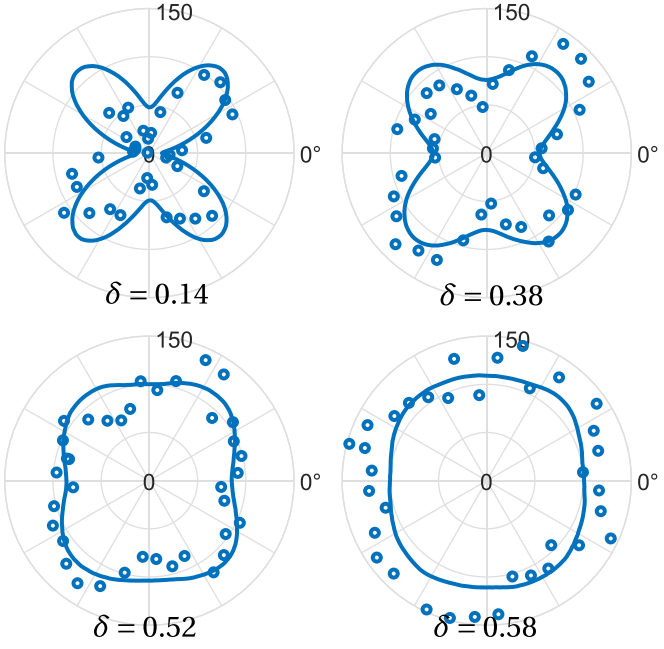

FIG. 5. Number of photons counted per 1000 laser shots in the wavelength range 450 ± 20 nm emitted in the plane perpendicular to laser propagation. Measurements of $\perp$ polarization for different elliptical laser polarization states are shown, all with peak laser field strength $a_0 = 1.52 \pm 0.08$. The data are compared with theoretical simulations (solid line) using the model described in Ref. [18] with an ensemble of 10 000 electrons randomly positioned in the laser focus.

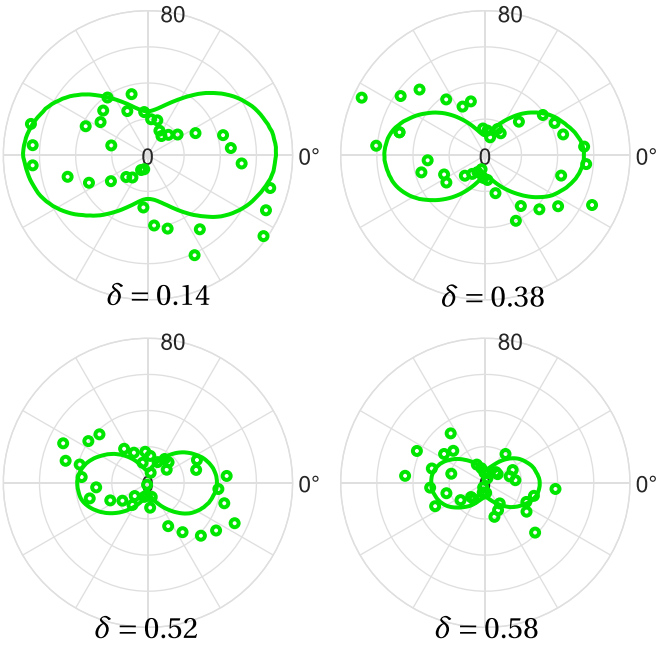

FIG. 6. Number of photons counted per 1000 laser shots in the wavelength range 450 ± 20 nm emitted in the plane perpendicular to laser propagation. Measurements of z polarization for different elliptical laser polarization states are shown, all with peak laser field strength $a_0 = 1.52 \pm 0.08$. The data are compared with theoretical simulations (solid line) using the model described in Ref. [18] for an ensemble of 10 000 electrons randomly positioned in the laser focus.

four graphs in Fig. 4. Errors in the measurement are at least as great as the asymmetries in the data reflected through the origin. Errors may be due to fluctuations and drift in laser parameters during the approximately 1 h required to collect data for one graph. Other errors might arise from an interplay between unknown focal distortions and the orientation of the polarization state. In spite of this, good qualitative agreement is seen between experiment and calculation for the different elliptical states.

The perpendicular component of the radiation pattern for a nearly linearly polarized laser ($\delta = 0.14$) is a dipole pattern with maxima perpendicular to the laser polarization, as expected. As the laser polarization state approaches circular, the initial dipole pattern evolves towards a circular shape. This can be understood as the introduction of more circular symmetry to the system, requiring the radiation pattern to become more circularly symmetric. We also see this in the trajectories in Figs. 3(a) and 3(b). The first term in Eq. (3a) has a contribution solely from $\dot{\boldsymbol{\beta}}_\perp$. For near-linear polarization, the acceleration is primarily in one dimension, and as a result the radiation pattern is an approximate dipole for the first harmonic. For elliptical states with higher δ, the acceleration is averaged more evenly in both the x and y directions, and thus, the instantaneous dipole is averaged in all directions. We note that, because perfect circular polarization was not achieved, the dipole pattern persists to a degree.

The number of scattered photons detected per 1000 laser shots for the second harmonic is displayed in Figs. 5 and 6, which show the $\perp$ and z components of the field. The helium pressure was 9.6×10^{-3} Torr. The theoretical curves in Figs. 5 and 6 are adjusted to match the data using a single overall normalizing factor that is the same for all graphs. Good qualitative agreement is found between the experiment and the model for the relative intensity scalings. Again, the transition from a case of lower symmetry with nearly linearly polarized light to a case of higher symmetry is reflected in the radiation pattern. The four-peaked pattern for the $\perp$ component discussed in Sec. II flattens to a near-circular pattern. The number of scattered photons remains relatively constant during the transition from nearly linear toward circular polarization states. For the second harmonic, the small overlap between the $\mathbf{n} \times (\mathbf{n} \times \dot{\boldsymbol{\beta}}_\perp)$ pattern and the $3\mathbf{n} \cdot \boldsymbol{\beta}_\perp$ pattern is increased as they both become more circular, counteracting the increased angular distribution of energy.

The z case for the second harmonic (Fig. 6) arises only because of the nonlinear trajectory and is a measurement of the z motion of the electron. The angular pattern of the z component of scattered second-harmonic light varies markedly between the case of an unfocused plane-wave pulse and a focused laser pulse. (Compare z polarization in Figs. 1 and 6.) In the latter case, the radiative pattern is elongated along the direction of linear polarization, as electrons oscillate in the presence of a strong ponderomotive gradient. Additionally, the strength of the emission does not fall off as fast when polarization states move toward circular. These focal-gradient effects are seen in both the experimental data and the theoretical simulations. The extent to which this might be used to characterize focal geometry as well as to distinguish between elliptical and perfectly circular polarization states is an interesting question.

V. CONCLUSION

The study of nonlinear Thomson scattering is rich with interesting harmonic coupling and radiation behaviors. In this work, we have considered in depth the origin of the harmonic radiation pattern for high-intensity laser fields of arbitrary elliptical polarization. Predictions of theoretical models described half a century ago were experimentally tested and analyzed. Both polarizations along the equator of the radiation sphere, $\perp$ and z, were measured. It was found that the circular symmetry of the radiation pattern increases with increased circularity of the driving laser for $\perp$ components of the radiation. The nonlinear radiation pattern and polarization are, in general, different from the linear case. This is primarily due to the fact that the electron acquires an oscillatory motion in the z direction from its relativistic transverse motion. When observed from the equator of the radiation sphere, the z motion induces z components in the emitted radiation. Unlike the $\perp$ component of radiation that is present in linear Thomson scattering, the z component is solely a nonlinear phenomenon. Additionally, the compression and stretching of the radiated wave fronts, due to the electron's relativistic motion, are crucial to understanding the radiation patterns. We explicitly observed the nonlinear z component radiation pattern for various elliptically polarized laser fields and showed that the theoretical model was in good agreement with experimental results. Our findings, and the polarization-resolved experimental techniques used to reconstruct the electron's trajectory, help describe how high-intensity laser fields interact with electrons.

Our confirmation of the theoretical model allows it to be used to predict arbitrary and unique polarization states, with applications in the development of radiation sources. It was shown here that the nonlinearity of the interaction enables access to previously inaccessible polarization states. Additional parameters, such as laser ellipticity and observation angle, increase the degrees of freedom, which is useful when developing novel radiation sources. In the case of scattering from electron beams, the capability demonstrated here of creating unique polarization states will also extend to the generation of higher-frequency xuv and x-ray light. The effects of NTS from elliptically polarized light, coupled with the effect on the radiation due to the observation angle, could also impact interpretation of recent observations of the polarization state of the cosmic microwave background [24] because most theoretical considerations of the cosmic microwave background consider only linear Thomson scattering. However, we have shown that even a mild nonlinearity can substantially alter the polarization state of the scattered radiation.

ACKNOWLEDGMENTS

This material is based upon work supported by the U.S. Department of Energy (DOE), Office of Science, Fusion Energy Sciences, under Award No. DE-SC0021018: LaserNetUS initiative at the Extreme Light Laboratory. Additional support was provided by the U.S. Department of Energy, Office of Science, High-Energy Physics (HEP), under Award No. DE-SC0019421, and the National Science Foundation, under Grant No. 1708185. This report was prepared as an account of work sponsored by an agency of the U.S. Government. Neither the U.S. Government nor any agency thereof, nor any of their employees, makes any warranty, express or implied, or assumes any legal liability or responsibility for the accuracy, completeness, or usefulness of any information, apparatus, product, or process disclosed, or represents that its use would not infringe privately owned rights. Reference herein to any specific commercial product, process, or service by trade name, trademark, manufacturer, or otherwise does not necessarily constitute or imply its endorsement, recommendation, or favoring by the U.S. Government or any agency thereof. The views and opinions of authors expressed herein do not necessarily state or reflect those of the U.S. Government or any agency thereof. The authors would like to thank Dr. Salamin and Dr. Carbajo for insightful conversations and the laser team at Extreme Light Laboratory for there tireless effort.

[1] D. M. Volkov, Über eine Klasse von Lösungen der Diracschen Gleichung, Z. Phys. **94**, 250 (1935).

[2] L. D. Landau and E. M. Lifshitz, *The Classical Theory of Fields* (Addison-Wesley, Cambridge, 1951), pp. 120–121.

[3] Vachaspati, Harmonics in the scattering of light by free electrons, Phys. Rev. **128**, 664 (1962).

[4] J. H. Eberly and A. Sleeper, Trajectory and mass shift of a classical electron in a radiation pulse, Phys. Rev. **176**, 1570 (1968).

[5] E. S. Sarachik and G. T. Schappert, Classical theory of the scattering of intense laser radiation by free electrons, Phys. Rev. D **1**, 2738 (1970).

[6] E. Esarey, S. K. Ride, and P. Sprangle, Nonlinear Thomson scattering of intense laser pulses from beams and plasmas, Phys. Rev. E **48**, 3003 (1993).

[7] Y. I. Salamin and F. H. M. Faisal, Harmonic generation by superintense light scattering from relativistic electrons, Phys. Rev. A **54**, 4383 (1996).

[8] T. J. Englert and E. A. Rinehart, Second-harmonic photons from the interaction of free electrons with intense laser radiation, Phys. Rev. A **28**, 1539 (1983).

[9] M. Iinuma, K. Matsukado, I. Endo, M. Hashida, K. Hayashi, A. Kohara, F. Matsumoto, Y. Nakanishi, S. Sakabe, S. Shimizu, T. Tauchi, K. Yamamoto, and T. Takahashi, Observation of second harmonics in laser–electron scattering using low energy electron beam, Phys. Lett. A **346**, 255 (2005).

[10] S. Chen, A. Maksimchuk, and D. P. Umstadter, Experimental observation of relativistic nonlinear Thomson scattering, Nature (London) **396**, 653 (1998).

[11] T. Kumita, Y. Kamiya, M. Babzien, I. Ben-Zvi, K. Kusche, I. V. Pavlishin, I. V. Pogorelsky, D. P. Siddons, V. Yakimenko, T. Hirose, T. Omori, J. Urakawa, K. Yokoya, D. Cline, and F. Zhou, Observation of the nonlinear effect in relativistic Thomson scattering of electron and laser beams, Laser Phys. **16**, 267 (2006).

[12] M. Babzien, I. Ben-Zvi, K. Kusche, I. V. Pavlishin, I. V. Pogorelsky, D. P. Siddons, V. Yakimenko, D. Cline, F. Zhou, T. Hirose, Y. Kamiya, T. Kumita, T. Omori, J. Urakawa, and K. Yokoya, Observation of the Second Harmonic in Thomson Scattering from Relativistic Electrons, Phys. Rev. Lett. **96**, 054802 (2006).

[13] A. Jochmann, A. Irman, M. Bussmann, J. P. Couperus, T. E. Cowan, A. D. Debus, M. Kuntzsch, K. W. D. Ledingham, U. Lehnert, R. Sauerbrey, H. P. Schlenvoigt, D. Seipt, Th. Stöhlker, D. B. Thorn, S. Trotsenko, A. Wagner, and U. Schramm, High Resolution Energy-Angle Correlation Measurement of Hard X Rays from Laser-Thomson Backscattering, Phys. Rev. Lett. **111**, 114803 (2013).

[14] K. Ta Phuoc, A. Rousse, M. Pittman, J. P. Rousseau, V. Malka, S. Fritzler, D. Umstadter, and D. Hulin, X-Ray Radiation from Nonlinear Thomson Scattering of an Intense Femtosecond Laser on Relativistic Electrons in a Helium Plasma, Phys. Rev. Lett. **91**, 195001 (2003).

[15] G. Sarri, D. J. Corvan, W. Schumaker, J. M. Cole, A. Di Piazza, H. Ahmed, C. Harvey, C. H. Keitel, K. Krushelnick, S. P. D. Mangles, Z. Najmudin, D. Symes, A. G. R. Thomas, M. Yeung, Z. Zhao, and M. Zepf, Ultrahigh Brilliance Multi-MeV γ-Ray Beams from Nonlinear Relativistic Thomson Scattering, Phys. Rev. Lett. **113**, 224801 (2014).

[16] W. Yan, C. Fruhling, G. Golovin, D. Haden, J. Luo, P. Zhang, B. Zhao, J. Zhang, C. Liu, M. Chen, S. Chen, S. Banerjee, and D. P. Umstadter, High-order multiphoton Thomson scattering, Nat. Photonics **11**, 514 (2017).

[17] J. M. Cole *et al.*, Experimental Evidence of Radiation Reaction in the Collision of a High-Intensity Laser Pulse with a Laser-

Wakefield Accelerated Electron Beam, Phys. Rev. X **8**, 011020 (2018).

[18] B. Pratt, N. Atkinson, D. Hodge, M. Romero, C. Schulzke, Y. Sun, M. Ware, and J. Peatross, Experimental confirmation of electron figure-8 motion in a strong laser field, Phys. Rev. A **103**, L031102 (2021).

[19] K. Krajewska, F. Cajiao Vélez, and J. Z. Kamiński, Control of relativistic ionization by polarization of short laser pulses, Europhys. Lett. **119**, 13001 (2017).

[20] N. Chen, T.-J. Wang, Z. Zhu, H. Guo, Y. Liu, F. Yin, H. Sun, Y. Leng, and R. Li, Laser ellipticity-dependent supercontinuum generation by femtosecond laser filamentation in air, Opt. Lett. **45**, 4444 (2020).

[21] J. E. Felten and P. Morrison, Recoil Photons from Scattering of Starlight by Relativistic Electrons, Phys. Rev. Lett. **10**, 453 (1963).

[22] J. E. Felten and P. Morrison, Omnidirectional inverse Compton and synchrotron radiation from cosmic distributions of fast electrons and thermal photons, Astrophys. J. **146**, 686 (1966).

[23] E. Feenberg and H. Primakoff, Interaction of cosmic-ray primaries with sunlight and starlight, Phys. Rev. **73**, 449 (1948).

[24] Y. Minami and E. Komatsu, New Extraction of the Cosmic Birefringence from the Planck 2018 Polarization Data, Phys. Rev. Lett. **125**, 221301 (2020).

[25] J. D. Jackson, *Classical Electrodynamics* (Wiley, New York, 1999), pp. 661–707.